Novel image analysis technique decodes the physiological information engraved on stratum corneum

Takeshi Tohgasaki[1*]; Saki Aihara[1]; Mariko Ikeda[1]; Shioji Ishiwatari[1]; Masaya Eto[2]; Riki Kudo[2]; Ai Kido[2]; Shinya Kondo[1]; Tetsuhito Sakurai[1]

[1] FANCL Research Institute, FANCL Corporation, 12-13 Kamishinano, Totsuka-ku, Yokohama, Kanagawa, Japan

[2] Software and AI Technology Center, Toshiba Digital Solutions Corporation, 72-34 Horikawa cho, saiwai-ku, Kawasaki, Kanagawa, JAPAN

* Corresponding author:Takeshi Tohgasaki, togasaki_takeshi@fancl.co.jp

Abstract

Background: Stratum corneum (SC) cells are imprinted with congenital and acquired physiological information; however, there is no method available to fully access and interpret this information. Therefore, the aim of this study was to develop a method for comprehensively decoding the physiological information of the skin included in SC cells. Toward this end, we established a novel image analysis technique based on artificial intelligence (AI) and multivariate analysis to estimate the skin condition.

Methods: SC samples were collected, imaged, and annotated to SC cells. Nine biomarkers in SC samples were measured using enzyme-linked immunosorbent assay. The data were then used to establish two machine learning models to automatically recognize individual SC cell regions in images and estimate the levels of the nine biomarkers. Skin physiological indicators (e.g., skin barrier function, facial analysis, questionnaire) were measured or obtained from self-report of the subjects. Multivariate analysis including biomarker levels and structural parameters of SC cells as variables was used to estimate these physiological indicators.

Results: We established two machine learning model. The accuracy of recognition was assessed according to the union average intersection (0.613), recall (0.953), accuracy (0.640), and F value (0.766). Biomarker levels predicted by the model significantly correlated with measured levels. Skin physiological indicators and the questionnaire answers were estimated with high correlation and correct answer rates.

Conclusion: Various skin physiological conditions can be estimated from SC cells using AI models and multivariate analysis. Our method is expected to be useful in optimization of treatment with a personalized approach.

Keywords: (Stratum Corneum, Machine learning, Multivariate analysis)

Introduction

The American architect Luis Sullivan is attributed to coining the phrase “form follows function,” which if correct, further implies that “function is inferred from form.” Based on this concept, the morphology of stratum corneum (SC) cells would follow skin physiological function. Indeed, the structure of SC cells is closely related to skin function such as skin barrier function, skin permeability, and nerve elongation [1-4]. SC cells are formed in the process of keratinization from the basement membrane to the surface layer. In the stratum granulosum, keratinocytes taken on a flattened morphology, forming a flat Kelvin tetradecahedron with tight junctions (TJs) to fill the spaces, exhibiting regular overlap and arrangement; the TJs and nucleus eventually disappear, leading to the final keratinization structure [5-7]. Therefore, a large amount of physiological information is engraved on the SC. Various methods have been proposed for evaluating skin physiological conditions based on the morphological characteristics of keratinocytes and the specific protein content in the SC. The area of SC cells was suggested as an index of the differentiation rate, and the exfoliation state of the SC was proposed as an index of the water content in the SC [8]. Moreover, we previously reported that specific protein expression levels in SC cells are associated with atopic dermatitis and skin barrier properties [9-14], and can be used as a biomarker for evaluating the skin condition. However, morphological evaluation of SC cells requires visual judgment and recognition, and biomarker measurement in SC cells requires a biochemical assay such as

immunoblotting or enzyme-linked immunosorbent assay (ELISA). These approaches require time, additional costs, and specific sophisticated equipment, which are barriers to the practical application and research of an appropriate evaluation method, necessitating the development of simple methods. Furthermore, there have been limited comprehensive studies on the morphological characteristics of SC cells, with much room for improvement in the evaluation method of the skin physiological state based on the morphological characteristics of SC cells. Machine learning technology has dramatically developed in recent years, enabling accurate recognition and classification of specific objects in images [15, 16], which has been applied in various fields such as in the analysis of microscopic and medical images [17, 18].

In this study, we constructed two machine learning models that automatically recognize individual SC cells and estimate the levels of relevant biomarkers in SC cells from images of SC cells. In addition, we developed a system for estimating skin physiological indicators and skin responsiveness by multiple regression analysis using the numerical output values from these two machine learning methods.

Materials and Methods

Subjects

We obtained data from two groups of subjects. SC cells from 996 healthy Japanese women (20–92 years old, average 43.2 years old) were collected and used as training data and test data to construct the machine learning model. In addition, to construct a mathematical model for estimating the physiological parameters of the skin, we collected SC cells, measured skin physiological parameters (see Sections below), and obtained responses from skin-related questionnaires from a separate group of 516 Japanese women (20–92 years old, average 44.3 years old). Written informed consent was obtained from all the subjects. The studies were conducted with t approval of the ethical committee of FANCL Co. Ltd. and as per the principles of the Declaration of Helsinki.

Collection and imaging of SC cells

SC samples of the cheek were obtained by single stripping using a skin tape (25 × 25 mm; Horney Layer Checker; Asahi Biomed Co. Ltd, Tokyo, Japan). The collected SC cells were imaged using Dino-lite AM7515 (AnMo Electronics Corp., Taiwan) with 8-bit RGB, 0.41μm/pixel, and the 2592 × 1944 pixels. Images were taken in 2–5 fields per

sample.

Data preparation for machine learning

We constructed two machine learning models: an automatic recognition model of individual SC cell regions and an estimation model of biomarker levels in the SC cells. Individual SC cell regions in images obtained from 996 subjects were visually identified and labeled using the annotation software Labelme (MIT, Cambridge, MA, USA) (Figure 1). In addition, the annotated images were expanded by rotation and inversion, which were used as the training and test images. For machine learning, an instance segmentation model pre-learned with ImageNet was used, and a machine learning model that automatically recognized individual SC cell regions was constructed. To construct a biomarker estimation model in the SC cells, 157 samples were used for the actual measurement and learning of the biomarker values. The model was trained based on the levels of nine biomarkers [heat shock protein 27 (HSP27), macrophage migration inhibitory factor (MIF), interleukin 1 receptor antagonist (IL-1Ra), DJ-1, galectin-7 (GAL-7), arginase-1 (ARG1), neutrophil gelatinase-associated lipocalin (NGAL), epidermal fatty acid binding protein (FABP5), and enolase-1 (Eno-1)] that were quantified using ELISA (see Section below) and the SC cell images. A convolutional neural network (CNN) was used for learning and a machine learning model for estimating biomarker values from the SC images was constructed.

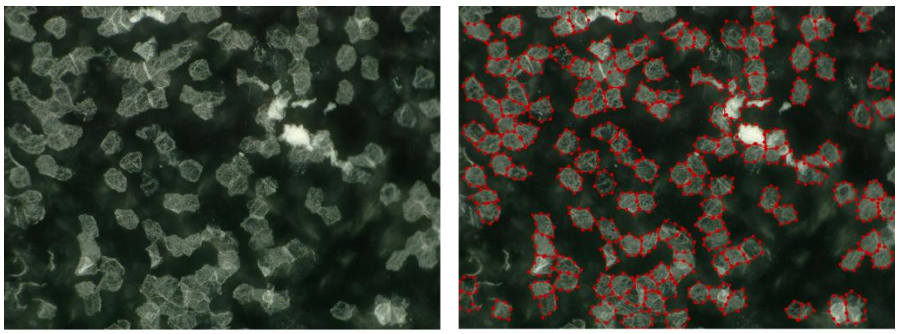

Figure 1 Annotation of SC cells from images
Raw image (left) and annotated data (right). The red frame indicates an SC region recognized by human sight.

ELISA

Samples were extracted using T-PER Tissue Protein Extraction Reagent (Thermo Fisher Scientific Inc., Waltham, MA, USA) or RIPA Lysis and Extraction Buffer

(Thermo Fisher Scientific). The concentrations of the nine biomarkers in the extracts were quantified using ELISA. To correct for the variable numbers of SC cells collected, total protein concentrations in the extracts were determined using the Pierce BCA Protein Assay Kit (Thermo Fisher Scientific) and the amount of biomarker per total protein was calculated. Machine learning was performed using this corrected value.

Quantification of SC cell shape

For SC cells in each image, individual cell regions were labeled using the automatic cell recognition model constructed in this study. The morphological parameters (area, circumference, roundness, regular polygon approximation, etc.) and intensity values (intracellular brightness mean, standard deviation, etc.) of each labeled cell were quantified. In addition, the variability in the shape and brightness values between the cells in the image was calculated. All cell regions and stratified regions were labeled using Otsu's method [19] for document image binarization, and these areas were quantified (Figure 2).

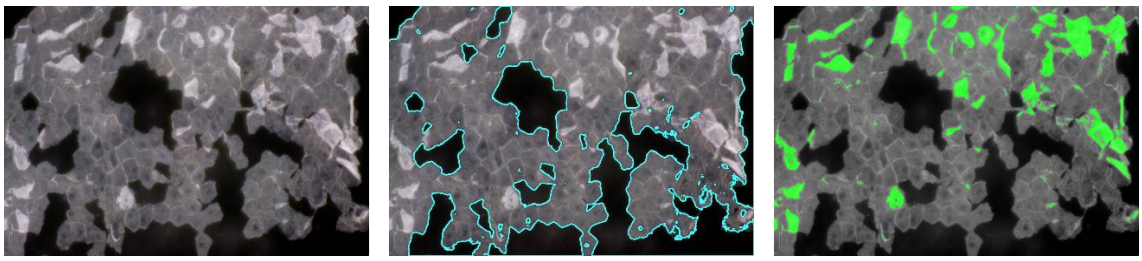

Figure 2 Identification of the cell region and multi-layered region by binarization. Raw image (left). All SC cell regions (center) and stratified regions (right) were labeled using Otsu's method. The blue line indicates the boundary between the cell area and the background, and the green area indicates the stratified regions.

Instruments and measurements

The skin parameters were assessed using noninvasive bioengineering measurements. The Tewameter VapoMeter (Keystone Scientific, Tokyo, Japan), SKICON 200EX skin conductance meter (Yayoi Co., Ltd., Tokyo, Japan) and MPA580 Cutometer® (Courage + Khazaka Electronic GmbH, Cologne, Germany) were used to determine trans-epidermal water loss (TEWL), skin hydration, and skin elasticity, respectively. Clinical images were taken using a VISIA evolution system (Canfield Scientific, Fairfield, New York, USA). The room used for measurements was kept at a constant temperature (21–24 °C) and within a certain humidity range (40–60%).

Questionnaires

The following questions related to the participants' skin response to cosmetics and ultraviolet (UV) radiation were asked: I. Cosmetics do not agree with your skin (yes/no); II. Experience inflammation and itching caused by cosmetics (very often/often/no); III. Reddening after sunburn (yes/no); IV. Turning brown after sunburn (yes/no).

Statistical analysis

Correlation analysis was performed using the Pearson product-moment correlation test to evaluate biomarker levels predicted by the machine learning model. To estimate skin parameters, multiple regression analysis was performed using structural and biomarker values as explanatory variables. Discriminant analysis was used to predict qualitative variables of the questionnaire answers. All statistical analyses were performed using JMP® 16.2.0 (SAS Institute Inc., Cary, NC, USA). Results were considered significant when $P < 0.05$.

Results

Machine learning model for automatic recognition of individual SC cell regions

First, we established two machine learning models that recognize SC cells regions and predict biomarker protein levels from SC images, respectively. A system that automatically recognizes SC cell regions was constructed by machine learning on a large number of SC cell images and their annotated images. To evaluate the accuracy of the automatic recognition model of the SC cell region, the machine-learning model was applied to the test data (not used to learn) for estimation of the SC cell region. The predicted images were merged with annotated data (Figure 3) and evaluated qualitatively and quantitatively. The number of cells recognized by the model was lower than that annotated by human visual judgment. In addition, the estimated cell region coincided approximately with the annotated region. Quantitative analysis showed that the intersection over union (IoU), recall, precision, and F-measure (F-number) was 0.613, 0.953, 0.640, and 0.766, respectively. Thus, recall was very high, whereas the IoU seemed to be reduced compared to visual evaluation.

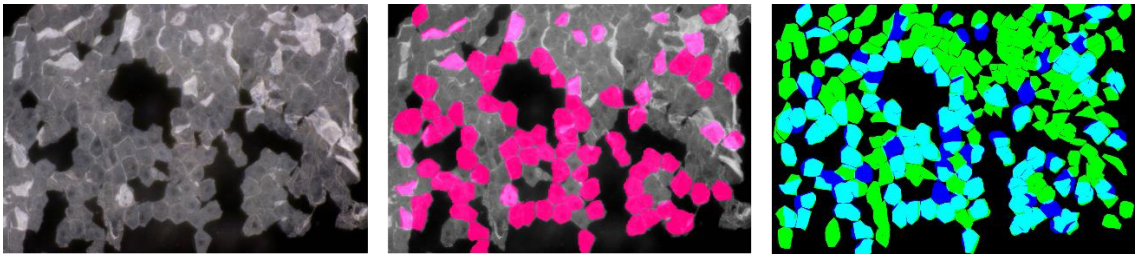

Figure 3 Evaluation of predicted and annotated regions
Raw image (left). Regions predicted by the machine-learning model (center); the pink area indicates the predicted region. Merged image (right); green: annotated area (false negative), blue: predicted area (false positive), cyan: true positive.

Machine learning model for estimating the biomarker levels of SC cells

We also constructed a model to estimate the levels of the nine biomarkers in the SC cells. To evaluate the accuracy of the biomarker estimation model, a machine learning model was applied to the test data to estimate the biomarker value. Correlation analysis was performed to evaluate the relationship between the values measured by ELISA and the predicted value, which showed that the predicted values of the nine biomarkers significantly correlated with the measured values, although the correlations were weak, with a correlation coefficient ranging from 0.213 to 0.450 (Figure 4). However, the predicted values of all markers were lower than the measured values and the distribution ranges were narrower.

Estimating skin physiological indicators from SC images

Next, we investigated whether it is feasible to estimate the skin physiological indicators by instrument measurement using the images of SC cells. The above two machine learning models were applied to SC cell images. The morphological parameters and brightness values of each labeled SC cell were also quantified. Multiple regression analysis was performed to predict the skin physiological indicators using the SC cell morphological parameters and biomarker levels predicted by the machine learning model as explanatory variables. The measured values of the SC water content and TEWL were significantly correlated with the estimated values from the multiple regression analysis (Figure 5). In particular, IL-1Ra, GAL-7, and ARG-1 levels and elliptic approximation contributed significantly to the estimation of SC water content, while HSP27, GAL-7, and DJ-1 levels, and cell circumference contributed significantly to the estimation of TEWL. The values of the elasticity indicators R0, R2, R5, R6, and R7 all showed a significantly strong correlation with the estimated values (Figure 6). HSP27 and DJ-1

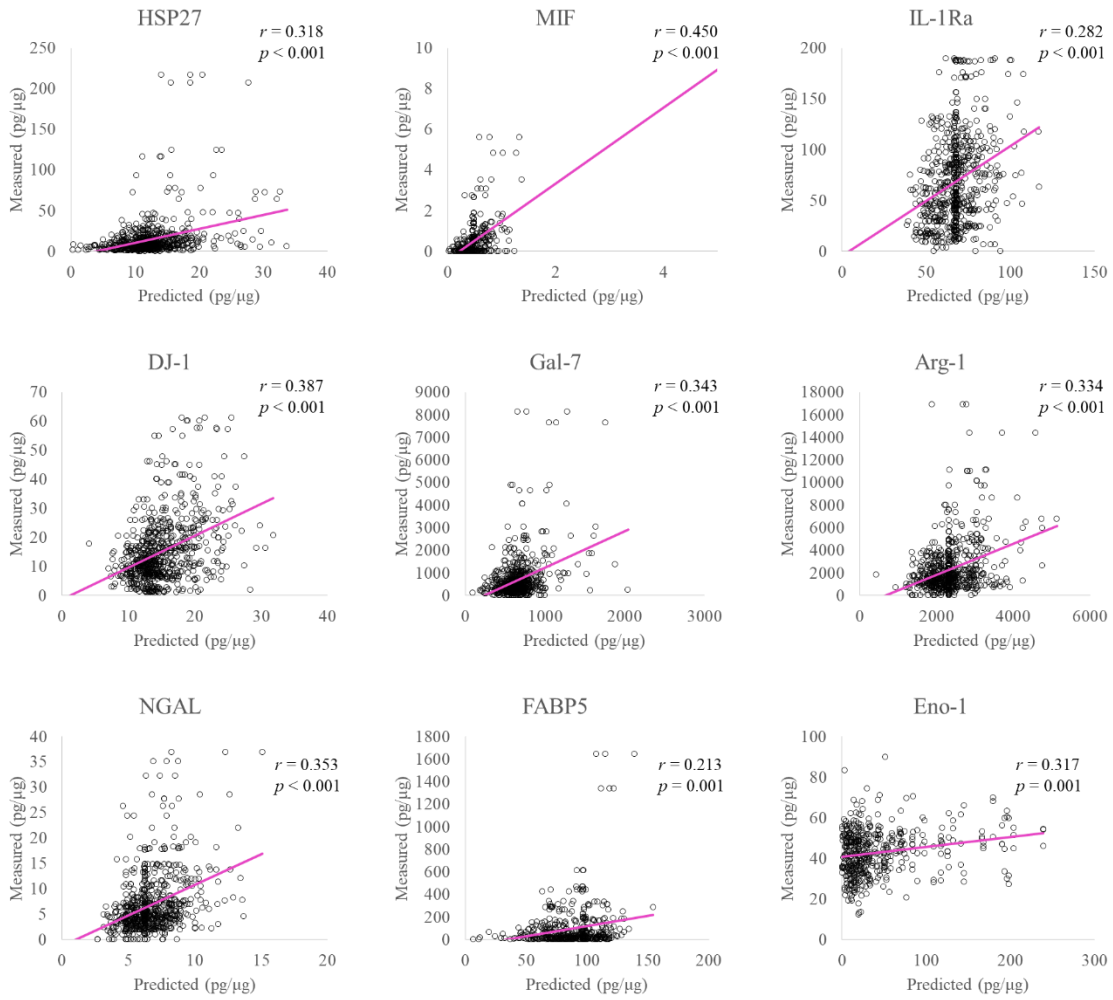

Figure 4 Correlation plots of predicted values determined by the machine-learning model and the values measured by ELISA for nine biomarkers in SC cells.

levels, the intracellular intensity value (average), and the long-short side ratio of a rectangle circumscribing a cell (average) were found to have high common contributions to these parameters. Indicators related to skin elasticity and wrinkles (texture count and wrinkle count), UV damage (UV spots), stains (brown spot count), pores (pore count and spot count), and to inflammation (red spot count and red vascular count) were output from the whole-facial imaging device VISIA, and a significant and strong correlation was obtained for each index (Figure 7). GAL-7 and ARG-1 levels, the long-short side ratio of a rectangle circumscribing a cell (average), and mean intracellular intensity values were highly correlated with indicators related to elasticity and wrinkles. The MIF and DJ-1

levels and number of angles of a regular polygon to approximate (standard deviation) were highly correlated with the UV damage index. HSP27 and MIF levels, number of angles of a regular polygon to approximate (average), and intracellular intensity value (average) were highly correlated with the brown spots. NGAL, ARG-1, and cell circumference (average) were closely associated with the pore index. HSP27, MIF, and area of the rectangle circumscribing the cell (average) were highly correlated with the index related to spots. IL-1Ra, DJ-1, and number of angles of a regular polygon to approximate (average) were highly correlated with indicators of inflammation. Table 1 shows the top 10 parameters with high contributions to predicting each indicator with the associated *t* value.

Estimating skin responsiveness from SC images

We verified the feasibility and accuracy of estimating the responsiveness of cosmetics and UV rays to the skin, as reported in the questionnaires, with the images of the SC cells. The questionnaire answers were predicted by discriminant analysis using the SC cell morphological parameters and biomarker levels estimated by the machine learning model as explanatory variables. Figure 8 shows the distribution ratios of the estimated and actual answers. It was possible to estimate whether cosmetics did not agree with the skin, with a correct answer rate of 84.3%. Regarding the experience of inflammation or itch caused by cosmetics, the overall correct rate was 57.9%, which was relatively low; however, for the answer “very often,” the correct rate was 78.3%, and when classified by experience or not, the correct rate was 72.4%. For the answers indicating that the skin turned red or black due to UV exposure, the correct rates were 70.9% and 68.5%, respectively.

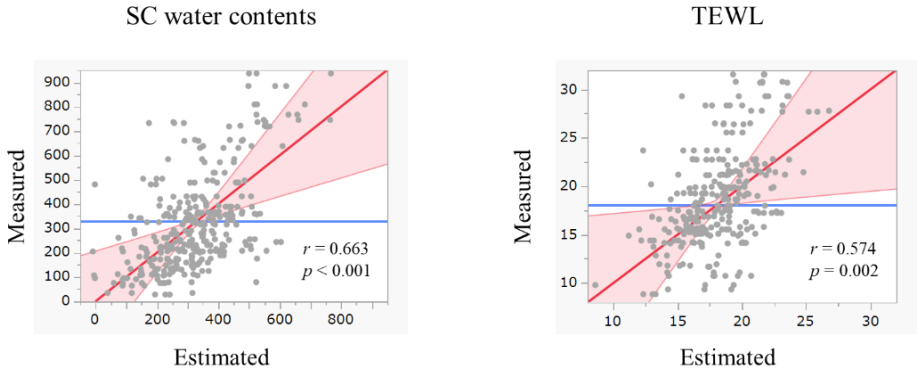

Figure 5 Correlation plots of predicted and measured values of SC water contents and TEWL

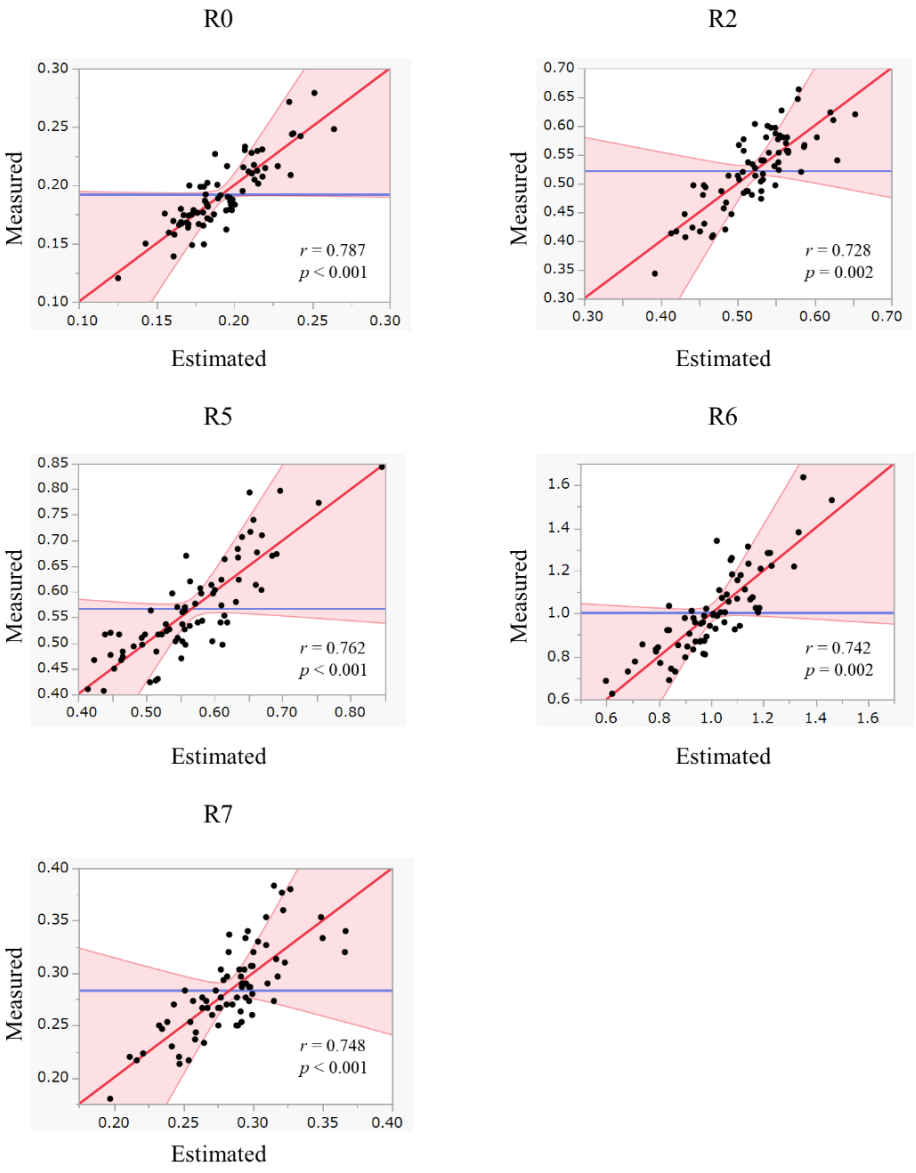

Figure 6 Correlation plots of predicted and measured values of elasticity indicators

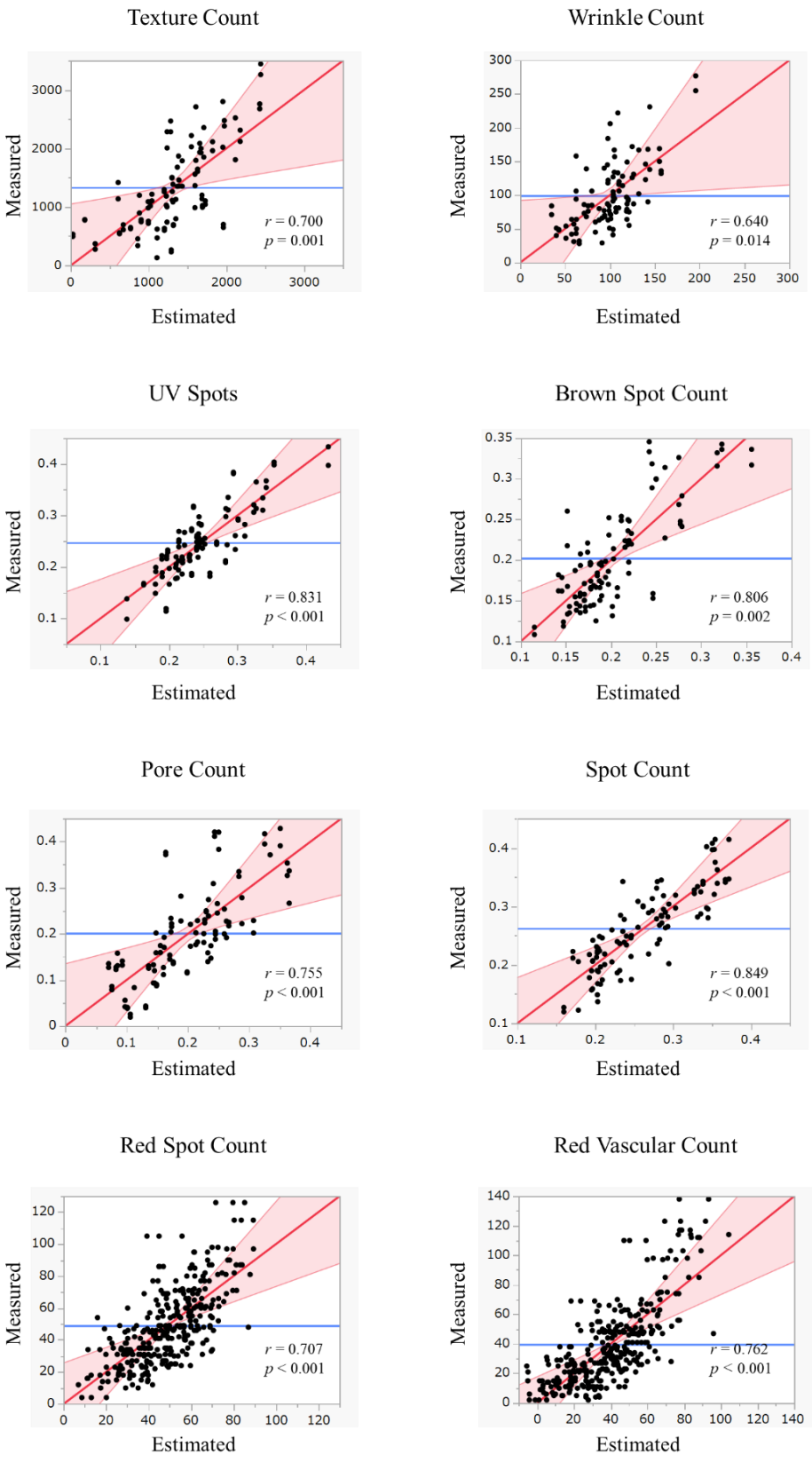

Figure 7 Correlation plots of predicted and measured values from VISIA

SC water content		TEWL		R0		R2		R5		R6		R7		Texture Count		Wrinkle Count		UV Spots		Brown Spot Count		Pore Count		Spot Count		Red spot Count		Red Vascular count	
Parameter	*t* value	Parameter	*t* value	Parameter	*t* value	Parameter	*t* value	Parameter	*t* value	Parameter	*t* value	Parameter	*t* value	Parameter	*t* value	Parameter	*t* value	Parameter	*t* value	Parameter	*t* value	Parameter	*t* value	Parameter	*t* value	Parameter	*t* value	Parameter	*t* value
IL-1RA	-2.89	HSP27	-2.95	Gal7	4.73	Intracellular intensity value (average)	3.66	Intracellular intensity value (average)	4.37	cell circumference (average)	3.79	Intracellular intensity value (average)	4.05	Long-short side ratio of a rectangle circumscribing a cell	-0.91	Long-short side ratio of a rectangle circumscribing a cell	-3.2	Number of angles of a regular polygon to approximate (standard	5.08	MIF	4.79	NGAL	3.97	Area of the rectangle circumscribing the cell (average)	-4.44	IL-1Ra	-2.65	Hsp27	5.08
Arg1	2.49	Gal7	2.94	Long-short side ratio of a rectangle circumscribing a cell	-4.27	Roundness (standard deviation)	-3.03	MIF	-3.31	DJ-1	-3.51	Cell circumference (standard deviation)	3.47	Intracellular brightness value (average)	-2.54	Intracellular brightness value (average)	-2.91	Intracellular brightness value (standard deviation)	-4.63	HSP27	-4.46	cell circumference (average)	3.63	MIF	3.72	Arg1	2.45	IL-1Ra	-4.63
iptic approximati	2.24	cell circumference (average)	-2.85	Intracellular intensity value (average)	-3.44	Long-short side ratio of a rectangle circumscribing a cell	3	HSP27	2.99	Cell area (average)	-2.24	HSP27	3.45	Gal7	2.22	Gal7	2.43	Number of angles of a regular polygon to approximate (average)	-4.58	NGAL	-3.97	Arg1	2.9	HSP27	-3.56	DJ-1	-2.35	Number of angles of a regular polygon to approximate (average)	-4.58
Gal7	-2.14	DJ-1	-2.65	Roundness (standard deviation)	3.4	Cell circumference (standard deviation)	2.88	Standard deviation of intracellular intensity value (average)	-2.68	Roundness (average)	2.15	MIF	-2.74	Arg1	2.92	Arg1	2.01	Intracellular brightness value (average)	-3.56	Number of angles of a regular polygon to approximate (average)	-3.88	Cell area (average)	-2.74	cell circumference (average)	3.12	Number of angles of a regular polygon to approximate (average)	-2.14	DJ-1	-3.56
NGAL	1.11	IL-1Ra	-2.38	Standard deviation of intracellular intensity value (average)	3.24	HSP27	2.76	Long-short side ratio of a rectangle circumscribing a cell	2.54	Standard deviation of intracellular intensity value (average)	-2.09	Number of angles of a regular polygon to approximate (average)	2.74	Cell circumference (standard deviation)	0.98	Cell circumference (standard deviation)	2.01	HSP27	-3.17	Intracellular brightness value (average)	-3.69	Cell circumference (standard deviation)	2.52	Gal7	3.09	cell circumference (average)	-1.88	Standard deviation of intracellular brightness value (standard	-3.17
Intracellular intensity value (average)	-1.07	Cell area (average)	2.11	Number of angles of a regular polygon to approximate (standard	-2.94	MIF	-2.57	Cell circumference (standard deviation)	2.47	Number of angles of a regular polygon to approximate (standard	1.67	Long-short side ratio of a rectangle circumscribing a cell	2.57	DJ-1	-2.45	DJ-1	-1.79	Area of the rectangle circumscribing the cell (average)	-3.06	Gal7	3.48	Roundness (average)	1.99	Number of angles of a regular polygon to approximate (average)	-3.06	NGAL	-1.74	NGAL	-3.06
Intracellular intensity value (standard diviation)	0.92	iptic approximati	1.92	Cell circumference (standard deviation)	-2.69	DJ-1	2.46	Number of angles of a regular polygon to approximate (average)	2.34	MIF	-1.46	DJ-1	2.52	Cell area (standard deviation)	0.06	Cell area (standard deviation)	-1.64	MIF	2.71	Area of the rectangle circumscribing the cell (average)	-3.45	MIF	-1.74	Intracellular brightness value (average)	-2.89	Roundness (average)	1.54	MIF	2.71
Cell area (average)	0.91	Arg1	1.44	DJ-1	2.49	Number of angles of a regular polygon to approximate (average)	2.44	Standard deviation of intracellular intensity value (standard	-2.14	Cell area (standard deviation)	1.44	Cell area (standard deviation)	-2.51	HSP27	-1.42	HSP27	-1.57	Gal7	2.46	Number of angles of a regular polygon to approximate (standard	2.5	DJ-1	-1.59	Roundness (standard deviation)	-2.15	HSP27	-1.45	Arg-1	2.46
DJ-1	-0.88	Minimum Intracellular intensity value (average)	-1.29	Intracellular intensity value (standard deviation)	2.43	Standard deviation of intracellular intensity value (average)	-2.32	Roundness (standard deviation)	-1.99	Arg1	1.4	Area of the rectangle circumscribing the cell (average)	2.14	cell circumference (average)	3.96	cell circumference (average)	1.3	NGAL	-2.45	Intracellular brightness value (standard deviation)	-2.34	Gal7	1.47	Cell circumference (standard deviation)	1.51	Area of the rectangle circumscribing the cell (average)	-1.32	Roundness (standard deviation)	2.09
cell circumference (average)	-0.58	Roundness (average)	1.28	HSP27	-2.29	Area of the rectangle circumscribing the cell (average)	2.26	Gal7	-1.69	Intracellular intensity value (standard deviation)	-1.21	Standard deviation of intracellular intensity value (standard	-2.12	Number of angles of a regular polygon to approximate (average)	-2.08	Number of angles of a regular polygon to approximate (average)	-1.11	Roundness (standard deviation)	2.09	Arg1	-2.21	Standard deviation of intracellular brightness value	-1.35	Cell area (standard deviation)	-1.49	Long-short side ratio of a rectangle circumscribing a cell	-1.22	Cell area (average)	1.65

Table 1 High contribution parameter (top 10) and *t* value

Experience that cosmetics don't agree with your skin.

		Predicted	
		NO	YES
Answer	NO	85%	15%
	YES	17%	84%

Experience that inflammation and itching caused by cosmetics.

		Predicted		
		NO	often	Very often
Answer	NO	64%	30%	6%
	often	33%	42%	25%
	Very often	8%	14%	78%

Turns red after sunburn.

		Predicted	
		NO	YES
Answer	NO	72%	28%
	YES	30%	71%

Turns brown after sunburn.

		Predicted	
		NO	YES
Answer	NO	65%	35%
	YES	28%	72%

Figure 8 Distribution ratio of the estimated answer and the actual answer

Discussion

In this study, we first developed two machine learning models: one that automatically recognizes individual SC cell regions in an image and another that predicts the levels of biomarkers in the SC from the image. The SC cell regions were recognized using this model with very high recall accuracy, although IoU and precision were low. However, since IoU was calculated including the area of the cells that the model did not recognize, the SC cells recognized by this model were actually recognized at a higher IoU. To evaluate the individual morphological characteristics of SC cells, it is necessary to accurately determine the morphology of typical cells, even in small numbers. Therefore, the recall and IoU values have a higher priority than precision. The model constructed in this study can automatically recognize the approximate SC cell morphological features. Visual judgment and annotation usually take approximately 1 h for one SC cell image, whereas our model can complete this task within a few seconds. This method would therefore be useful for real-time skin evaluation and abundant sample evaluations. We also attempted machine learning to determine the presence of nuclei in the SC cells; however, the recognition accuracy was only 45% (data not shown), and further learning was required.

The model for estimating biomarker levels roughly predicted the measured levels quantified by ELISA. A weak but significant correlation was confirmed between the model-predicted levels and measured levels of the biomarkers. However, the estimated levels were smaller than the measured values, and their distribution was narrow. This may indicate that the training data were biased in terms of the median values; thus, it would be necessary to train the data with a wide distribution uniformly. Measuring biomarkers in SC cells requires extensive time, money, and equipment. Moreover, there are also limits to the types of biomarkers that can be measured from a single sample. Our machine-learning model can easily and quickly determine the approximate number of multiple markers without these limitations. There is room for further improvement in estimation accuracy when adding training data, optimizing the imaging device and settings, and optimizing the module in machine learning. Moreover, multiple regression analysis with the predicted values and SC cell morphological parameters has potential to improve the estimation accuracy.

Next, using the morphological parameters and biomarker levels of the SC cells from the two constructed machine-learning models, verification of the skin physiological state was performed by multiple regression analysis and discriminant analysis. Our data showed that the SC water content, TEWL, elasticity value, and index from VISIA could be estimated from image analysis of SC cells, with high correlations obtained. Furthermore, the results of questionnaires regarding cosmetics and UV responsiveness could be estimated with correct rates of 70–85% by analysis of SC cells.

The relationship between SC cell characteristics and the physiological state of the skin has been studied for a long time, and some methods have been developed that are used in clinical settings. Our two machine-learning models for images of SC cells offers a convenient approach to obtain SC cell morphological parameters and nine biomarker levels. Thus, we could comprehensively and quickly quantify the characteristics of the SC cells, which can help progress research into understanding the relationship between the characteristics of SC cells and the skin physiological condition. In this study, we clarified the relationship with several physiological indicators; however, there is potential to estimate many other physiological indicators, future skin conditions, and to predict the effects of cosmetics by analyzing SC cells. Furthermore, multiple regression analysis can be used to identify biomarkers or morphological parameters that are highly correlated with each skin physiological state among many parameters. These parameters are useful for elucidating the mechanisms underlying skin physiology. For example, relationships between HSP27 and GAL-7 in the SC cells and barrier indicators, SC water content, and TEWL have been reported [12, 14]. Our data also suggest that these relationships are particularly stronger than those of other parameters. Conversely, we found that the non-uniformity of the intensity of the SC cells, which has not been paid attention to in the past, is highly related to the pore index. We identified a large number of such relationships, which may provide key information for the discovery of new dermatological mechanisms. Thus, our image analysis technique can help to decode the enormous amount of information engraved in SC cells beyond what is possible to observe with the naked eye.

Conclusion

We constructed two machine-learning models that can automatically recognize SC cells

and estimate the biomarkers levels in SC cells. The barrier function, color, inflammation, elasticity, and responsiveness of the skin can be estimated by the morphological characteristics and biomarker levels of the SC cells output by these models. Various skin physiological conditions can be identified from the analysis of SC cells by machine learning with image and multivariate analyses.

Acknowledgments

This work was supported by a grant awarded by the FANCL Corporation.

Conflict of Interest Statement

NONE

References

[1] M. Tominaga, H. Ogawa, K. Takamori, Decreased production of semaphorin 3A in the lesional skin of atopic dermatitis, Br J Dermatol 158(4) (2008) 842-4.

[2] S. Takahashi, A. Ishida, A. Kubo, H. Kawasaki, S. Ochiai, M. Nakayama, H. Koseki, M. Amagai, T. Okada, Homeostatic pruning and activity of epidermal nerves are dysregulated in barrier-impaired skin during chronic itch development, Sci Rep 9(1) (2019) 8625.

[3] M. Machado, T.M. Salgado, J. Hadgraft, M.E. Lane, The relationship between transepidermal water loss and skin permeability, Int J Pharm 384(1-2) (2010) 73-7.

[4] A. Kubo, K. Nagao, M. Amagai, Epidermal barrier dysfunction and cutaneous sensitization in atopic diseases, J Clin Invest 122(2) (2012) 440-7.

[5] M. Yokouchi, T. Atsugi, M.V. Logtestijn, R.J. Tanaka, M. Kajimura, M. Suematsu, M. Furuse, M. Amagai, A. Kubo, Epidermal cell turnover across tight junctions based on Kelvin's tetrakaidecahedron cell shape, Elife 5 (2016).

[6] K. Yoshida, M. Yokouchi, K. Nagao, K. Ishii, M. Amagai, A. Kubo, Functional tight junction barrier localizes in the second layer of the stratum granulosum of human epidermis, J Dermatol Sci 71(2) (2013) 89-99.

[7] T. Sugawara, N. Iwamoto, M. Akashi, T. Kojima, J. Hisatsune, M. Sugai, M. Furuse, Tight junction dysfunction in the stratum granulosum leads to aberrant stratum corneum barrier function in claudin-1-deficient mice, J Dermatol Sci 70(1) (2013) 12-8.

[8] N.O. Nobuo Kashibuchi, Masakazu Miyazawa, Norio Fujiwara,, Y.H. Atsushi Kishita, The Relationship between Sensitive Skin and Stratum Corneum Morphology, Journal of Society of Cosmetic Chemists of Japan 33 (1999) 290-296.

[9] Y. Yamane, K. Moriyama, C. Yasuda, S. Miyata, M. Aihara, Z. Ikezawa, K. Miyazaki, New horny layer marker proteins for evaluating skin condition in atopic dermatitis, Int Arch Allergy Immunol 150(1) (2009) 89-101.
[10] C. Yasuda, A. Enomoto, S. Ishiwatari, N. Mori, K. Kagoyama, K. Matsunaga, Y. Yoshihisa, S. Matsukuma, T. Shimizu, Macrophage migration inhibitory factor (MIF) in the stratum corneum: a marker of the local severity of atopic dermatitis, Exp Dermatol 23(10) (2014) 764-6.
[11] S. Ishiwatari, M. Takahashi, C. Yasuda, M. Nakagawa, Y. Saito, N. Noguchi, S. Matsukuma, The protective role of DJ-1 in ultraviolet-induced damage of human skin: DJ-1 levels in the stratum corneum as an indicator of antioxidative defense, Arch Dermatol Res 307(10) (2015) 925-35.
[12] S. Niiyama, T. Yoshino, C. Yasuda, X. Yu, R. Izumi, S. Ishiwatari, S. Matsukuma, H. Mukai, Galectin-7 in the stratum corneum: a biomarker of the skin barrier function, Int J Cosmet Sci 38(5) (2016) 487-95.
[13] T. Tohgasaki, N. Ozawa, T. Yoshino, S. Ishiwatari, S. Matsukuma, S. Yanagi, H. Fukuda, Enolase-1 expression in the stratum corneum is elevated with parakeratosis of atopic dermatitis and disrupts the cellular tight junction barrier in keratinocytes, Int J Cosmet Sci 40(2) (2018) 178-186.
[14] S. Niiyama, T. Yoshino, S. Matsukuma, H. Mukai, Heat Shock Protein 27 kDa Content in Stratum Corneum Correlates with Severity of Atopic Dermatitis, Acta Derm Venereol 96(7) (2016) 976-977.
[15] A. Krizhevsky, I. Sutskever, G.E. Hinton, ImageNet classification with deep convolutional neural networks, Proceedings of the 25th International Conference on Neural Information Processing Systems - Volume 1, Curran Associates Inc., Lake Tahoe, Nevada, 2012, pp. 1097–1105.
[16] M.D. Zeiler, R. Fergus, Visualizing and Understanding Convolutional Networks, Springer International Publishing, Cham, 2014, pp. 818-833.
[17] G. Quellec, G. Cazuguel, B. Cochener, M. Lamard, Multiple-Instance Learning for Medical Image and Video Analysis, IEEE Rev Biomed Eng 10 (2017) 213-234.
[18] A. Kar, M. Petit, Y. Refahi, G. Cerutti, C. Godin, J. Traas, Benchmarking of deep learning algorithms for 3D instance segmentation of confocal image datasets, PLoS Comput Biol 18(4) (2022) e1009879.
[19] N. Otsu, A Threshold Selection Method from Gray-Level Histograms, IEEE Transactions on Systems, Man, and Cybernetics 9(1) (1979) 62-66.